RSC Advances

COMMUNICATION

View Article Online
View Journal | View Issue

Cite this: *RSC Adv.*, 2015, **5**, 57700

The hydrogenation of aromatic-naphthalene with Ni_2P/CNTs

Minzhi Ruan,[a] Jun Guan,[a] Demin He,[a] Tao Meng[c] and Qiumin Zhang*[ab]

Received 26th March 2015
Accepted 16th June 2015

DOI: 10.1039/c5ra05364a

www.rsc.org/advances

Ni_2P/CNTs was synthesized using an impregnation method. XPS revealed that CNTs could affect the electronic properties of bulk Ni_2P. The catalyst shows superior activity for HYD of naphthalene with a conversion of 99%, and demonstrates superior tolerance towards potential catalyst poisons, which is higher than Ni/CNTs with a conversion of 89%.

Due to the increasingly low quality of petroleum feedstocks and stringent environmental regulations, it is of paramount importance to develop new environmentally friendly catalysts for hydrotreatment. The hydrogenation (HYD) and hydrodesulfurization (HDS) reactions, which transfer polycyclic aromatic hydrocarbons with sulfur into high RON oil, underpin many clean-energy technologies. Although Pt or Pd have been used in hydrotreatment catalysts, they have poor performances when in contact with sulfur.[1] Furthermore Pt and Pd are luxurious and relatively infrequent in the Earth's shell limiting the use of them in energy systems deployed on a global scale. More recently, nanoparticulate films of Ni_2P composed of inexpensive materials to show high HDS activity. As the nickel phosphorus catalyst was firstly introduced by Oyama, it has aroused lots of interest all around the world as it has been used in energy applications with high performances of HDS and hydrodenitrogenation (HDN) activity and even has outstanding performances in fuel cells. This indicated that the sequence of HYD activity over transition metal phosphides is as follows: Fe_2P < CoP < MoP < WP < Ni_2P, where the Ni_2P catalyst was found to be the most active.[2–4] Among such classes of catalysts, various carbon nanostructures, including carbon, carbon nanotubes, and graphene and so on, have been used for catalyst carriers which have excellent performances.[5,6] However, carbon nanotubes (CNTs) with unique properties have experienced limited use as a support material for Ni_2P, and the potential industrial application value of Ni_2P/CNTs in aromatic HYD has not been sufficiently explored. Herein, we have thus applied Ni_2P catalysts supported on carbon nanotubes to examine the effect of HYD. CNTs was reported to have huge specific areas, therefore they have a better hydrogen storage function and strictly mesoporous nature, differing greatly from the classical activated carbon support.[7–13] The CNTs was functionalized using an acid mixture which led to the unique CNT properties, and the Ni_2P/CNTs particles were synthesized using an impregnation method.[14]

X-ray diffraction patterns of reduced Ni_2P/CNTs and Ni_2P samples are presented in Fig. 1a. The Ni_2P loadings were varied from 5 to 40 wt%, and the Ni/P mole ratios were varied from 0.5 to 2.0. With the increase of Ni_2P loadings and Ni/P mole ratios, the sharp and symmetric peaks evidently indicate that the samples were well crystallized. The patterns all display a broad feature at 20–30° and 48.8° due to the carbon nanotube supports. For all of the catalysts, the peaks at $2\theta = 40.6°$, 44.5°, 47.1°, 54.1°, 54.8° (PDF: 74-1385) can be ascribed to Ni_2P, and no additional phase of Ni and P is observed, indicating that the active phase formed is mainly Ni_2P. The 30 wt% Ni_2P/CNTs sample (Fig. 1b) was substantiated by energy dispersive spectroscopy (EDS) in Fig. 1c.

The IR spectrum of the acid-treated CNTs and Ni_2P/CNTs catalysts is shown in Fig. 1d. The bands appearing at 1000 cm^{-1} can be assigned to the Ni_2P, and the bands appearing at 1635 and 3450 cm^{-1} can be assigned to the C=O and O–H stretching vibration bands, which confirm the presence of functional groups in the acid-treated CNTs, and could help adsorb active metal on the surface.[15]

Table 1 shows the physical properties of the Ni_2P/CNTs catalysts, including the Ni_2P loading content, average Ni_2P size and BET surface area. The results showed that the BET surface area of the catalysts declined with the increase in the amount of Ni_2P loading. This indicated that the Ni_2P particles

[a]*School of Chemical Engineering, Dalian University of Technology (DUT), No. 2 Linggong Road, Dalian 116024, P. R. China. E-mail: zhangqm@dlut.edu.cn; Fax: +86 0411 84986150; Tel: +86 0411 84986150*

[b]*State Key Laboratory of Fine Chemicals, Dalian University of Technology (DUT), China*

[c]*Beijing Guodian Longyuan Environmental Engineering Co., LTD, Building No. 1, Yard No. 16, Xisihuan Mid Road, Haidian District, Beijing 100039, PR China*

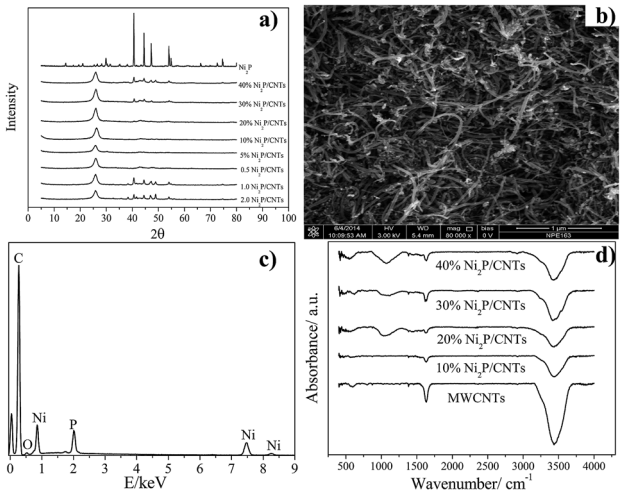

Fig. 1 (a) XRD patterns of catalyst samples with different wt% of Ni_2P (Ni/P = 1.25, atomic) and Ni/P proportion (30 wt% Ni_2P); (b) SEM image of 30 wt% Ni_2P/CNTs; (c) EDS of 30 wt% Ni_2P/CNTs; (d) FTIR of catalyst samples.

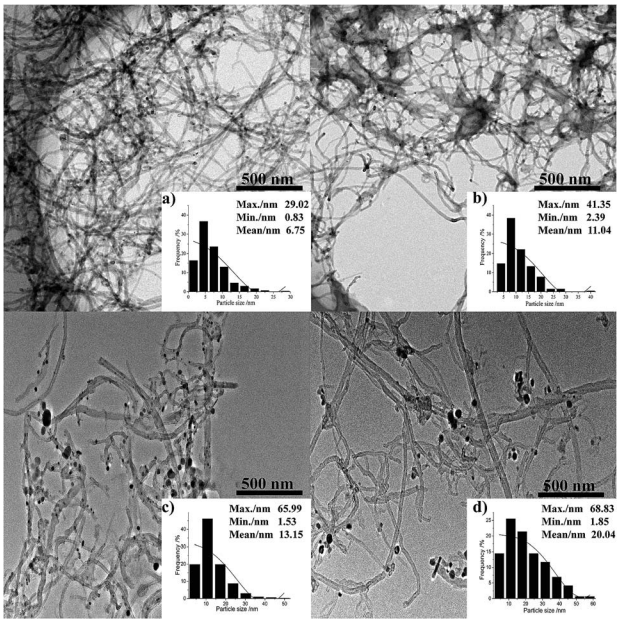

Fig. 2 TEM images and size distribution histograms: (a) 10 wt% Ni_2P/CNTs, (b) 20 wt% Ni_2P/CNTs, (c) 30 wt% Ni_2P/CNTs and (d) 40 wt% Ni_2P/CNTs.

occupied the surface holes of the CNTs. TEM observations indicate that the size and the morphology of the Ni_2P/CNTs composites differ from those of the CNTs. Most of the Ni_2P particles are displayed outside of the CNTs, the loading content could affect the Ni particle size and its distribution.[15] In addition, as the histograms in Fig. 2 show, the mean particle size increases from 6.7 nm to 20.0 nm with the increasing loading content. In the following section, it was found that a smaller Ni_2P particle size with a higher dispersion contributes to the inhibition of the agglomeration of Ni_2P particles, which should favour the hydrogenation reaction.

The XPS Ni 2p and P 2p spectra of 30 wt% Ni_2P/CNTs catalysts are presented in Fig. 3a and b. For samples (1)–(3), the Ni 2p core level spectrum includes two contributions (Fig. 3a and b), which correspond to Ni $2p_{3/2}$ and Ni $2p_{1/2}$, respectively. The former one, is assigned to $Ni^{\delta+}$ in the Ni 2p phase and is centered at 853.31 eV, and the later one at 857.9 eV is assigned to oxidized Ni. With regards to the P $2p_{3/2}$ binding energy, the peaks of the P 2p electron binding energy at 129.87 eV and 133.98 eV can be assigned to oxidized and elemental P, respectively.

The peaks in the XPS spectrum for the Ni_2P catalyst have been assigned previously.[16,17] For Ni_2P, the binding energies at 857.9 and 134.8 eV are assigned to Ni^{2+} and P^{5+} species. The XPS spectrum for the 30 wt% Ni_2P/CNTs catalyst commonly mirrors that of the Ni_2P catalyst. The fresh Ni_2P/CNTs sample displays two distinct peaks, whose positions correspond to the Ni–P and Ni–Ni distances in bulk Ni_2P. The P (2p) region shows one significant difference: the XPS spectrum of the Ni_2P catalyst has a very intense peak at 132.04 eV but there are two peaks in the XPS spectrum of Ni_2P/CNTs that are consistent with the binding energy for phosphorus in the CNTs. Some of the phosphorus impregnated onto the CNTs apparently reacts with the support to form Ni–P-CNTs. The spectrum of fresh Ni_2P/CNTs differs from the Ni_2P sample, indicating that the Ni^+ peak shifted from 855.4 to 853.31 eV (Fig. 3a), and the binding energy assigned to the P^{5+} species shifted from 131.96 to 129.87 eV (Fig. 3b). The shift of binding energies of the surface Ni^+ and P^{5+} species suggests the existence of an electronic effect caused by the surface –OH or –COOH, or CNTs species, which may result in the electron enrichment of the surface Ni and P species. As it is revealed in Fig. 3c and d, the Ni atom is placed on an atop site instead of at a hole site, there are two stable binding sites for a Ni_2 dimer on a carbon nanotube wall: an atop–atop site and a bridge–bridge site. The Ni_2 dimer when placed on a nanotube

Table 1 BET results and pore structure parameters of Ni_2P/CNTs catalysts

Samples	Surface area[a] ($m^2\ g^{-1}$)	Pore volume[a] ($cm^3\ g^{-1}$)	dXRD[b] (nm)	dTEM[c] (nm)
10 wt%	171	0.33	13.6	6.7
20 wt%	151	0.31	14.6	11.0
30 wt%	143	0.26	21.9	13.1
40 wt%	94	0.23	28.0	20.0

[a] Evaluated from N_2 adsorption–desorption isotherms. [b] Calculated using the Scherrer equation from the XRD. [c] Measured using TEM.

Table 2 Catalytic hydrogenation of naphthalene and 1-methyl naphthalene[a]

Samples	Raw materials	Products	Selectivity [%]
30 wt% Ni_2P/CNTs	Naphthalene	*cis*-Decalin	14
		trans-Decalin	69
		Tetralin	17
30 wt% Ni_2P/CNTs	1-Methyl naphthalene	1-Methyl tetralin	17
		5-Methyl tetralin	36
		1-Methyl decalin	47
20 wt% Ni/CNTs	Naphthalene	*cis*-Decalin	0
		trans-Decalin	28
		Tetralin	61

[a] Reaction conditions: reactions were carried out with naphthalene or 1-methyl naphthalene (5 wt% in decane), at 613 K, 4.0 MPa, vapour–liquid ratio = 600, LHSV = 4.0 h^{-1}. The Ni loading of 20 wt% Ni/CNTs is equal to the Ni loading of 30 wt% Ni_2P/CNTs. Reactions were carried out in a continuous-flow microreactor.

Table 3 Hydrotreatment performance of the Ni_2P/CNTs catalysts[a]

Entry	Ni_2P (wt%)	Ni/P (atomic)	LHSV (h^{-1})	Conversion [%]
1	40	1.25	4	91
2	30	1.25	4	>99
3	20	1.25	4	65
4	10	1.25	4	30

[a] Reaction conditions: reactions were carried out with naphthalene (5 wt%), at 613 K, 4.0 MPa.

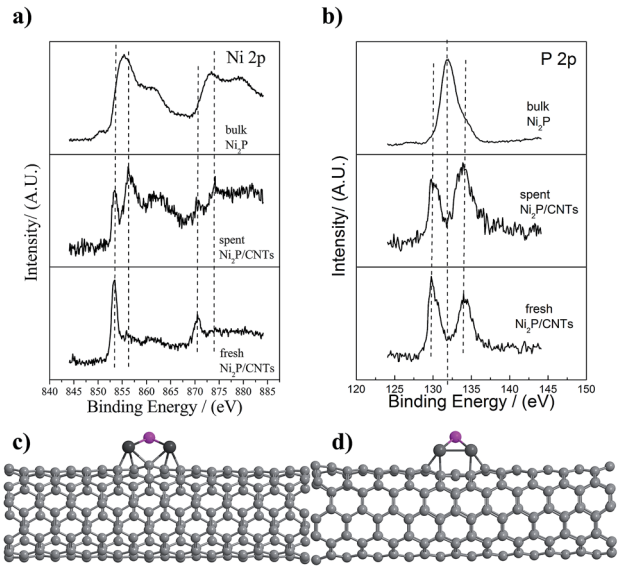

Fig. 3 XPS spectra for Ni_2P, spent Ni_2P/CNTs and fresh Ni_2P/CNTs: (a) Ni 2p core level spectra and (b) P 2p core level spectra. The two stable binding sites for Ni_2P on CNTs: (c) atop–atop site and (d) bridge–bridge site.

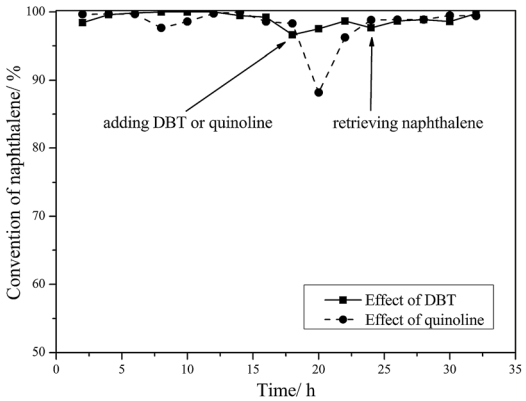

Fig. 4 Effect of adding DBT or quinolone to HYD. The content of HDS and HDN intermediates of DBT and quinoline was 1.0 wt% in 5.0 wt% naphthalene reactant.

wall has a tendency to separate in a reaction mediated by the underlying carbon atoms. Thus, the number of Ni_2 configurations on a tube varies with the curvature and Ni_2 exhibits a larger range of Ni–Ni bond lengths (2.34–2.78 Å).[18] A significant shift in binding energy peaks assigned to the spent phosphorus species in Ni_2P/CNTs was detected, illustrating that the addition of functionalized CNTs could affect the electronic properties of bulk Ni_2P.[19]

The hydrotreatment reaction results for Ni_2P/CNTs in the HYD of naphthalene and 1-methyl naphthalene are summarized in Tables 2 and 3. Mass balance is 100 ± 5% for each reaction type. The reaction of naphthalene on 30 wt% Ni_2P/CNTs (Ni/P = 1.25, mol) occurs with a very high and stable conversion of 99%, which is much higher than for the other samples or that of the Ni_2P/SiO_2 and NiP/C catalysts.[8,20] This may be attributed to 30 wt% Ni_2P/CNTs having a higher BET surface area which could provide more Ni_2P active sites on the surface of the CNTs (Table 1), furthermore, the Ni_2P particles of the 30 wt% samples with a small size were well dispersed on the CNTs (Fig. 2). There are three major products formed from naphthalene on these catalysts: *cis*-decalin, *trans*-decalin and tetralin, compared with the Ni_2P/SiO_2 catalysts, Ni_2P/CNTs gave a higher *trans*-decalin selectivity of 69% and the proportion of *cis*-decalin and *trans*-decalin is nearly 1 : 4, indicating that it favours the hydrogenation pathway. In comparison with

naphthalene, tetralin, the final product of HYD of 1-methyl naphthalene is less than 50%, this is due to the steric hindrance effect caused by the methyl group. The Ni/CNTs catalyst exhibits less activity with a conversion of 84%. Obviously, the existence of P contributes to the HYD; the joint action of the Ni–P-CNTs effect could be explained by the XPS results. Liu *et al.* also confirmed that the P sites of the phosphide of Ni_2P play a complex and significant role. First, the Ni–P bonds produce a weak ligand effect that allows a reasonably high activity of HYD. Second, the amount of Ni active sites on the surface decreases owing to an ensemble effect of P, which prevents the reaction system from deactivating. Third, the P sites are spectators and provide moderate bonding and the H adatoms are essential for HYD.[21]

We next investigated the durability and the resistance to sulfur and nitrogen solutions of the catalysts. As revealed in Fig. 4, after contact with the sulfur and nitrogen solutions, the initial HYD conversion dropped from 99% to 85%, however when the solution was switched to naphthalene, the catalyst can return to its former level, demonstrating superior tolerance towards potential catalyst poisons, such as DBT and quinoline.

In summary, a novel Ni_2P/CNTs catalyst was developed for HYD. The catalyst exhibited excellent activity and stability, and was successfully used for HDS or HDN, showing superior performance to a Pt–Pd catalyst. As aromatic compounds are important components of fuels, this work is a significant step towards the development of more active and practical catalysts for the upgrading of coal-tar and bio-oil.

Experimental section

Multi-carbon nanotubes were purchased from CAS (Chengdu, China). Concentrated nitric acid (70%, Aladdin) was used to functionalize the CNTs at 60 °C for 6 h. Nickel phosphate compounds loaded with CNTs were prepared by the following route: nickel nitrate (60 mg, 99%, Aladdin) and ammonium hydrogen phosphate (20 mg, 99%, Aladdin) were dissolved in deionized water. Functionalized CNTs (100 mg) were then mixed into the solution. Ultrasonication was carried out for 6 h and followed by impregnation at room temperature. The sample was then collected and calcined in N_2 at 793 K. Reduction was conducted in 95% H_2 mixed with 5% He with a total flow of 100 mL min^{-1} at 793 K. Subsequently, the calcined sample was pelletized and sieved for the HYD reaction.

Acknowledgements

The authors thank the financial support of the Major Project of the National Energy Administration (NY20130302513-1).

Notes and references

1 H. Song, J. Wang, Z. Wang, H. Song, F. Li and Z. Jin, *J. Catal.*, 2014, **311**, 257.
2 S. T. Oyama, *J. Catal.*, 2003, **216**, 343.
3 A. Infantes-Molina, J. A. Cecilia, B. Pawelec, J. L. G. Fierro, E. Rodríguez-Castellón and A. Jiménez-López, *Appl. Catal., A*, 2010, **390**, 253.
4 J. Chang, L. Feng, C. Liu, W. Xing and X. Hu, *Angew. Chem., Int. Ed.*, 2014, **53**, 122.
5 Y. Shu and S. T. Oyama, *Carbon*, 2005, **43**, 1517.
6 Y. Lu, J. Tu, Q. Xiong, Y. Qiao, J. Zhang, C. Gu, X. Wang and S. X. Mao, *Chem.–Eur. J.*, 2012, **18**, 6031.
7 Y. Lu, X. Wang, Y. Mai, J. Xiang, H. Zhang, L. Li, C. Gu, J. Tu and S. X. Mao, *J. Phys. Chem. C*, 2012, **116**, 22217.
8 A. C. Dillon, K. M. Jones, T. A. Bekkedahl, C. H. Kiang, D. S. Bethune and M. J. Heben, *Nature*, 1997, **386**, 377–379; S. T. Oyama, X. Wang, Y. K. Lee and W. J. Chun, *J. Catal.*, 2004, **221**, 263.
9 E. G. Rodrigues, S. A. C. Carabineiro, J. J. Delgado, X. Chen, M. F. R. Pereira and J. J. M. Órfão, *J. Catal.*, 2012, **285**, 83–91.
10 F. Zhu, G. Ma, Z. Bai, R. Hang, B. Tang, Z. Zhang and X. Wang, *J. Power Sources*, 2013, **242**, 610–620.
11 D. Z. Mezalira and M. Bron, *J. Power Sources*, 2013, **231**, 113–121.
12 V. Lordi, N. Yao and J. Wei, *Chem. Mater.*, 2001, **13**, 733–737.
13 S. M. Bachilo, L. Balzano, J. E. Herrera, F. Pompeo, D. E. Resasco and R. B. Weisman, *J. Am. Chem. Soc.*, 2003, **125**, 11186–11187.
14 M. Moula, S. Suzuki, W. Chun, S. Otani, S. T. Oyama and K. Asakura, *Surf. Interface Anal.*, 2006, **38**, 1611.
15 M. Zhou, H. Zhu and L. Niu, *et al.*, *Catal. Lett.*, 2014, **144**(2), 235–241.
16 D. Kanama, *Surf. Sci. Spectra*, 2001, **8**, 220.
17 P. Liu, J. A. Rodriguez, Y. Takahashi and K. Nakamura, *J. Catal.*, 2009, **262**, 294.
18 M. Menon, A. N. Andriotis and G. E. Froudakis, *Chem. Phys. Lett.*, 2000, **320**, 425.
19 D. S. Misra, A. Misra, P. K. Tyagi and M. K. Singh, *Diamond Relat. Mater.*, 2006, **15**, 385.
20 S. Yang and R. Prins, *Chem. Commun.*, 2005, 4178.
21 P. Liu, J. A. Rodriguez and T. Asakura, *et al.*, *J. Phys. Chem. B*, 2005, **109**(10), 4575–4583.